Kinetic Studies of Reactions of Dioxygen with Carboxylate-Bridged Diiron(II) Complexes Leading to the Formation of (μ-Oxo)diiron(III) Complexes

Andrew L. Feig, Axel Masschelein, Andreja Bakac,[†] and Stephen J. Lippard*

Contribution from the Department of Chemistry, Massachusetts Institute of Technology, Cambridge, Massachusetts 02139

Received August 12, 1996[⊗]

Abstract: Stopped-flow kinetic studies of the reactions of [Fe₂(BIPhMe)₂(O₂CH)₄] (**1a**), where BIPhMe = 2,2′-bis-(1-methylimidazolyl)phenylmethoxymethane, and [Fe₂(OH)(Me₃TACN)₂(OAc)₂]⁺ (**2a**), where TACN = 1,4,7-trimethyl-1,4,7-triazacyclononane, with O_2 are presented. In $CHCl_3$, both reactions are first-order in $[O_2]$ and second-order in diiron(II) complex concentration. Mechanisms consistent with the kinetic data are proposed. The main feature of these schemes is a bimolecular pathway involving a tetranuclear ($μ^4$-peroxo)diiron(II)diiron(III) species in the transition state. Evidence for carboxylate shifts in the oxidation mechanisms is presented, offering one possible way in which this class of structural equilibria might control the chemistry at related non-heme diiron centers in metalloproteins.

Introduction

Hemerythrin (Hr),[1−3] the R2 subunit of ribonucleotide reductase (RNR),[4−7] Δ-9-desaturase,[8] and soluble methane monooxygenase (sMMO) hydroxylase[9−12] are members of an emerging class of non-heme carboxylate-bridged diiron proteins with important physiological roles.[2,13−15] Despite diverse biological functions, these proteins share a common structural motif and are all involved in reactions with dioxygen. The active centers of all four proteins contain pairs of iron atoms bridged by the carboxylate side chains of glutamate or aspartate. In their oxidized forms, additional monoatomic oxo or hydroxo bridges, depending on the protein, are also present. The terminal sites are occupied by nitrogen atoms from histidine and oxygen atoms from additional carboxylate ligands and water. The isolated enzymes generally contain iron in the +3 oxidation

state, but the metal centers must be reduced to the diiron(II) state to observe activity.

The nature of the non-carboxylate bridging ligand differs among these proteins. In the case of deoxyHr, a dioxygen transport protein from marine invertebrates, a hydroxide ion bridges the two iron atoms. A vacant coordination site present on one iron is available for dioxygen binding. This reaction is accompanied by two-electron oxidation of the diiron(II) center and proton transfer from the hydroxo bridge to the terminally coordinated peroxide. A hydrogen bond forms between the resulting hydroperoxide and the oxo bridge.[16] In the R2 protein, no monoatomic bridge is observed in the reduced state.[17] Upon reaction with dioxygen, however, a (μ-oxo)diiron(III) unit forms together with a functionally significant tyrosyl radical.[18−20] In sMMO hydroxylase, the bridging ligands vary with conditions. X-ray crystallographic studies have identified both (μ-hydroxo)-bis(μ-carboxylato)diiron(III) and (μ-hydroxo)(μ-aqua)(μ-carboxylato)diiron(III) cores.[10,21] In the reduced state, a bis(μ-carboxylato)diiron(II) center different from that of R2 is observed.[21] The core geometry of the reduced Δ-9-desaturase enzyme has just been determined.[8b]

Significant progress has been made in modeling both the diiron(II) and diiron(III) forms of these proteins.[14,22,23] These studies have afforded valuable structural, spectroscopic, and magnetic information, but only a few have focused on chemical reactivity, especially of diiron(II) with dioxygen.[15,24−28] Many of the important questions remaining to be answered for diiron

† Permanent address: Ames Laboratory, Iowa State University, Ames, Iowa 50011.
⊗ Abstract published in *Advance ACS Abstracts,* December 15, 1996.
(1) Stenkamp, R. E.; Sieker, L. C.; Jensen, L. H.; McCallum, J. D.; Sanders-Loehr, J. *Proc. Natl. Acad. Sci. U.S.A.* **1985,** *82,* 713−716.
(2) Sanders-Loehr, J. In *Iron Carriers and Iron Proteins*; Loehr, T. M., Ed.; VCH: New York, 1989; Vol. 5, pp 373−466.
(3) Stenkamp, R. E. *Chem. Rev.* **1994,** *94,* 714−726.
(4) Nordlund, P.; Sjöberg, B.-M.; Eklund, H. *Nature* **1990**, *345,* 593−598.
(5) Stubbe, J. In *Advances in Enzymology and Related Areas of Molecular Biology*; Meister, A., Ed.; John Wiley and Sons: New York, 1990; Vol. 62, pp 349−420.
(6) Stubbe, J. *J. Biol. Chem.* **1990,** *265,* 5329−5332.
(7) Fontecave, M.; Nordlund, P.; Eklund, H.; Reichard, P. In *Advances in Enzymology and Related Areas of Molecular Biology*; Meister, A., Ed.; Wiley and Sons: New York, 1992; Vol. 65, pp 147−183.
(8) (a) Fox, B. G.; Shanklin, J.; Somerville, C.; Münck, E. *Proc. Natl. Acad. Sci. U.S.A.* **1993,** *90,* 2486−2490. (b) Lindqvist, Y.; Huang, W.; Schneider, G.; Shanklin, J. *EMBO J.* **1996,** *15,* 4081−4092.
(9) Fox, B. G.; Froland, W. A.; Dege, J. E.; Lipscomb, J. D. *J. Biol. Chem.* **1989,** *264,* 10023−10033.
(10) Rosenzweig, A. C.; Frederick, C. A.; Lippard, S. J.; Nordlund, P. *Nature* **1993,** *366,* 537−543.
(11) Lipscomb, J. D. *Annu. Rev. Microbiol.* **1994,** *48,* 371−399.
(12) Liu, K. E.; Lippard, S. J. *Adv. Inorg. Chem.* **1995,** *42,* 263−289.
(13) Howard, J. B.; Rees, D. C. In *Advances in Protein Chemistry*; Anfinsen, C. B., Edsall, J. T., Richards, F. M., Eisenberg, D. S., Eds.; Academic: New York, 1991; Vol. 42, pp 199−280.
(14) Que, L., Jr. In *Bioinorganic Catalysis*; Reedijk, J., Ed.; Marcel Dekker: New York, 1993; pp 347−393.
(15) Feig, A. L.; Lippard, S. J. *Chem. Rev.* **1994,** *94,* 759−805.

(16) Shiemke, A. K.; Loehr, T. M.; Sanders-Loehr, J. *J. Am. Chem. Soc.* **1986,** *108,* 2437−2443.
(17) Logan, D. T.; Su, X.-D.; Åberg, A.; Regnström, K.; Hajdu, J.; Eklund, H.; Nordlund, P. *Structure* **1996,** *4,* 1053−1064.
(18) Tong, W. H.; Chen, S.; Lloyd, S. G.; Edmondson, D. E.; Huynh, B. H.; Stubbe, J. *J. Am. Chem. Soc.* **1996,** *118,* 2107−2108.
(19) Burdi, D.; Sturgeon, B. E.; Tong, W. H.; Stubbe, J.; Hoffman, B. M. *J. Am. Chem. Soc.* **1996,** *118,* 281−282.
(20) Sturgeon, B. E.; Burdi, D.; Chen, S.; Huynh, B.-H.; Edmonson, D. E.; Stubbe, J.; Hoffman, B. M. *J. Am. Chem. Soc.* **1996,** *118,* 7551−7557.
(21) Rosenzweig, A. C.; Nordlund, P.; Takahara, P. M.; Frederick, C. A.; Lippard, S. J. *Chem. Biol.* **1995,** *2,* 409−418.
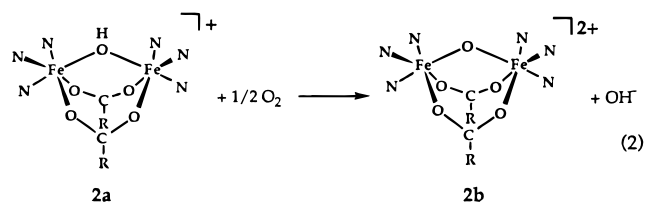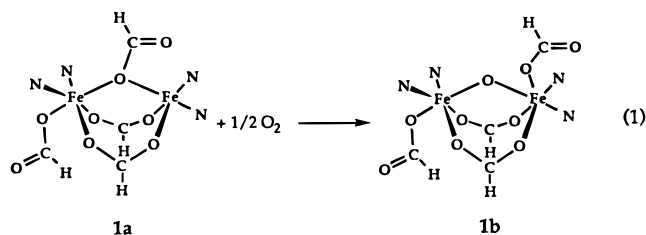(22) Kurtz, D. M., Jr. *Chem. Rev.* **1990,** *90,* 585−606.
(23) Herold, S.; Pence, L. E.; Lippard, S. J. *J. Am. Chem. Soc.* **1995,** *117,* 6134−6135.
(24) Feig, A. L.; Becker, M.; Schindler, S.; van Eldik, R.; Lippard, S. J. *Inorg. Chem.* **1996,** *35,* 2590−2601.

carboxylate systems can best be addressed by kinetic studies. Is the O−O or the C−H bond broken first in C−H activation? Which factors control the reversibility of O_2 binding? What intermediates are involved? These questions are important to address directly for the protein, but detailed mechanistic studies on well-characterized models are also of considerable value. Such studies lead to improved models and ultimately provide more information to help interpret results with the proteins.

Only a few relevant kinetic studies have been published on model compounds, and they concern ligand or bridge exchange reactions.[29,30] A detailed kinetic study of the autoxidation of cyclidene-based non-heme dioxygen carriers demonstrated the availability of an outer-sphere electron-transfer pathway when inner-sphere coordination of dioxygen was sterically prevented.[31-33] In other investigations, ferrous chelates generated in situ afforded a metastable diferric peroxide species.[34,35] Results of low-temperature kinetic studies on related reactions of dioxygen with a series of alkoxo-bridged compounds have been reported from our laboratory.[24,36] The reactions of dioxygen with metalloprotein active sites have also been investigated by Co(II) and Cu(I) model chemistry.[37-39]

In the present work, the reaction of dioxygen with two fully characterized diiron(II) model compounds has been studied. Both yield well-defined (μ-oxo)diiron(III) products, as shown in eqs 1 and 2. The reduced species are [Fe$_2$(BIPhMe)$_2$(O$_2$CH)$_4$] (**1a**),[40,41] where BIPhMe = 2,2′-bis(1-methylimidazolyl)phenylmethoxymethane, and [Fe$_2$(OH)(Me$_3$TACN)$_2$(OAc)$_2$](ClO$_4$) (**2a**),[42] Me$_3$TACN = 1,4,7-trimethyl-1,4,7-triazacyclononane. Upon reaction with dioxygen, these two complexes are oxidized in high yield (>95%) to [Fe$_2$O(BIPhMe)$_2$(O$_2$CH)$_4$] (**1b**) and [Fe$_2$O(Me$_3$TACN)$_2$(OAc)$_2$]$^{2+}$ (**2b**), respectively. Kinetic results were obtained by stopped-flow spectrometry. A portion of this work was previously described,[43] and it should be noted that, in this early discussion, the reaction order with respect to **1a** for eq 1 was incorrectly given.

(25) Dong, Y.; Yan, S.; Young, V. G., Jr.; Que, L., Jr. *Angew. Chem., Int. Ed. Engl.* **1996**, *35*, 618−620.

(26) Kim, K.; Lippard, S. J. *J. Am. Chem. Soc.* **1996**, *118*, 4914−4915.

(27) Que, L., Jr. *Acc. Chem. Res.* **1996**, *29*, 190−196.

(28) Ookubo, T.; Sugimoto, H.; Nagayama, T.; Masuda, H.; Sato, T.; Tanaka, K.; Maeda, Y.; Okawa, H.; Hayashi, Y.; Uehara, A.; Suzuki, M. *J. Am. Chem. Soc.* **1996**, *118*, 701−702.

(29) Drüeke, S.; Wieghardt, K.; Nuber, B.; Weiss, J.; Fleischhauer, H.-P.; Gehring, S.; Haase, W. *J. Am. Chem. Soc.* **1989**, *111*, 8622−8631.

(30) Watton, S. P.; Masschelein, A.; Rebek, J., Jr.; Lippard, S. J. *J. Am. Chem. Soc.* **1994**, *116*, 5196−5205.

(31) Dickerson, L. D.; Sauer-Masarwa, A.; Herron, N.; Fendrick, C. M.; Busch, D. H. *J. Am. Chem. Soc.* **1993**, *115*, 3623−3626.

(32) Sauer-Masarwa, A.; Dickerson, L. D.; Herron, N.; Busch, D. H. *Coord. Chem. Rev.* **1993**, *128*, 117−137.

(33) Busch, D. H.; Alcock, N. W. *Chem. Rev.* **1994**, *94*, 585−623.

(34) Purmal, A. P.; Skurlatov, Y. I.; Travin, S. O. *Izv. Akad. Nauk SSSR, Ser. Khim.* **1980**, *3*, 492−497.

(35) Nishida, Y.; Yoshizawa, K.; Takahashi, S. *J. Chem. Soc., Chem. Commun.* **1991**, 1647−1648.

(36) Feig, A.; Lippard, S. J. *J. Am. Chem. Soc.* **1994**, *116*, 8410−8411.

(37) Davies, R.; Stevenson, M. B.; Sykes, A. G. *J. Chem Soc. A* **1970**, 1261−1266.

(38) El-Sayed, M. A.; Ismail, K. Z.; El-Zayat, T. A.; Davies, G. *Inorg. Chim. Acta* **1994**, *217*, 109−119.

(39) Karlin, K. D.; Nasir, M. S.; Cohen, B. I.; Cruse, R. W.; Kaderli, S.; Zuberbuhler, A. D. *J. Am. Chem. Soc.* **1994**, *116*, 1324−1336.

(40) Tolman, W. B.; Bino, A.; Lippard, S. J. *J. Am. Chem. Soc.* **1989**, *111*, 8522−8523.

(41) Tolman, W. B.; Liu, S.; Bentsen, J. G.; Lippard, S. J. *J. Am. Chem. Soc.* **1991**, *113*, 152−164.

(42) Hartman, J. R.; Rardin, R. L.; Chaudhuri, P.; Pohl, K.; Wieghardt, K.; Nuber, B.; Weiss, J.; Papaefthymiou, G. C.; Frankel, R. B.; Lippard, S. J. *J. Am. Chem. Soc.* **1987**, *109*, 7387−7396.

(43) Liu, K. E.; Feig, A. L.; Goldberg, D. P.; Watton, S. P.; Lippard, S. J. In *The Activation of Dioxygen and Homogeneous Catalytic Oxidation*; Barton, D. H. R., Martell, A. E., Sawyer, D. T., Eds.; Plenum: New York, 1993; pp 301−320.

Experimental Section

Preparation and Characterization of Compounds. 2,2′-Bis(1-methylimidazolyl)phenylmethoxymethane (BIPhMe) and [Fe$_2$(BIPh-Me)$_2$(O$_2$CH)$_4$] (**1a**) were prepared as previously described.[40,41] 1,4,7-Trimethyl-1,4,7-triazacyclononane (Me$_3$TACN) was synthesized according to a published procedure,[44] except for the detosylation step, which was carried out in 30% HBr in glacial acetic acid at reflux for 48 h to yield 59.3% TACN·3HBr. This hydrobromide salt was used in the subsequent steps of the published procedure without further purification. [Fe$_2$(OH)(Me$_3$TACN)$_2$(OAc)$_2$](ClO$_4$) (**2a**) was synthesized as previously reported.[42,45] Dry methanol was prepared by distillation from Mg(OMe)$_2$, and dry chloroform was obtained by distillation from CaH$_2$ after predrying with activated 4 Å molecular sieves.

Stopped-Flow Kinetics Experiments. Two stopped-flow instruments were used in these experiments. Ambient temperature data (22 ± 1 °C) were collected by using an umbilical device, Applied Photophysics Rapid Kinetics Accessory RX-1000, fitted with Teflon flow lines and an argon-purged anaerobic attachment to avoid premature oxidation of air-sensitive solutions. Variable temperature data were collected with a Hi-Tech SF-41 Canterbury stopped-flow device fitted with Teflon-lined stainless steel flow lines. Once purged of dioxygen, these flow lines provided greater protection against premature oxidation and dioxygen leakage than standard Teflon lines and required no further purging with argon or nitrogen.

Optical absorption data were collected by using one of two independent detection systems depending on the time scale of the reaction. For reaction times greater than 1 min employing the RX-1000 device, a Hewlett-Packard 8452A diode array spectrometer was used, allowing collection of multiwavelength data. Spectra as a function of time from 300 to 820 nm and kinetic traces at single wavelengths were obtained. The resolution was 2 nm, and the fastest acquisition time was one spectrum every 2 s. For more rapid reactions and all experiments performed in the SF-41, a specially assembled fiber-optics spectrometer (components from Oriel Corp.) was used. This instrument has been described previously.[24] Data were analyzed with a statistical program (Kaleidagraph, Synergy Software) by nonlinear least-squares regression on model-dependent equations. All reactions were followed for at least 3 half-lives at wavelengths appropriate for the detection of the products.

Solutions for the stopped-flow experiments were prepared anaerobically in a nitrogen-filled glovebox (Vacuum Atmospheres) and loaded into gas-tight syringes (Hamilton) modified with Kel-F threaded adapters to fit the stopped-flow apparatus. Reaction orders with respect to the iron complexes were determined by the initial rate method,[46] by varying the concentration of the complex solution. Pseudo-order conditions with excess dioxygen (~5.7 mM in CHCl$_3$) were maintained

(44) Wieghardt, K.; Chaudhuri, P.; Nuber, B.; Weiss, J. *Inorg. Chem.* **1982**, *21*, 3086−3090.

(45) Chaudhuri, P.; Wieghardt, K.; Nuber, B.; Weiss, J. *Angew. Chem., Int. Ed. Engl.* **1985**, *24*, 778−779.

(46) Connors, K. A. *Chemical Kinetics. The Study of Reaction Rates in Solution*; VCH Publishers: New York, 1990.

in these experiments. Complex concentrations typically varied from 0.05 to 0.50 mM. Orders with respect to dioxygen were determined by saturating a reservoir containing pure solvent with a dioxygen/dinitrogen mixture. The O_2/N_2 ratio was controlled by the precise flow meters of a dynamic gas mixing system (Matheson, Inc.). The actual dioxygen concentrations in solution were calculated from Ostwald's coefficient of O_2 in the appropriate solvent and the mole ratio of the gas mixture.[47] Reaction orders were obtained from the slopes of the $\ln(k_\psi)$ versus $\ln([O_2])$ plots, where k_ψ is the pseudo-order rate constant. When other additives were present, they were introduced as part of the oxygenated solutions. All experiments were repeated at least twice. Dioxygen concentrations were adjusted for solvent contraction in the variable temperature work on the basis of a measured linear approximation of the solvent density.[48]

Manometric Analysis. Dioxygen uptake experiments in chloroform and methanol were conducted by using a mercury-filled U-tube manometer and a calibrated sample cell. A detailed description of the apparatus and procedure is reported elsewhere.[41] In brief, the sample was loaded into the cell as a solution in a known volume of solvent, usually 11 mL. After degassing the sample by three freeze−pump−thaw cycles, the manometer was charged with a known pressure of dioxygen. The system was isolated from the gas inlet, and the sample cell was opened to the manometer and allowed to equilibrate until the pressure remained constant. The change in pressure (ΔP) was corrected for dioxygen solubility in the solvent by subtracting the ΔP for a control reaction containing an equal volume of pure solvent and converted to moles of dioxygen on the basis of a measured calibration constant derived from the ideal gas law. No differences in dioxygen uptake were detected when the solvent was changed. Data are reported as the mean of three separate uptake experiments.

Resonance Raman Experiments. Solutions of **2a** (∼5 mM) in methanol were prepared in the glovebox in septum-sealed tubes. The samples were oxidized by addition of air or $^{18}O_2$ (91%) (Isotech). Spectra were recorded on an OMA III (EG&G PARC Model 1460) analyzer and an intensified diode-array detector (EG&G PARC Model 1455) attached to a 0.6 m single monochromator (SPEX, 2400 grooves/mm grating) with irradiation at 406.7 nm (Kr-ion laser, Coherent Innova 90-K). To determine whether OH^- exchanges with the oxo bridge, 2 M NaOH in MeOH was added dropwise to ^{18}O-labeled **2b**.

NMR Studies. Solutions of **2a** (5−10 mM) in deuterated solvents (CD_3OD or $CDCl_3$), or in ^1H solvents for ^2H NMR experiments, were prepared in a glovebox under a nitrogen atmosphere. The septum-sealed tubes were removed from the box and flame sealed. Spectra were collected on a Varian XL300 spectrometer with a multinuclear probe. Temperatures were calibrated by using pure samples of methanol and the internal calibration routine of the instrument. Sweep widths of 1000−1333 ppm were scanned for features before focusing on individual peaks. Spectra were externally referenced to pure solvent or to tetramethylsilane.

Triphenylphosphine Oxidation. The possibility that triphenylphosphine might be oxidized to triphenylphosphine oxide was assayed by either GC (HP-5890, 12 m × 0.2 mm × 0.2 μm HP-101 column, fluid phase methyl silicone) or ^{31}P NMR spectroscopy. In a typical experiment, anaerobic solutions of the diiron(II) complex were prepared in the glovebox in the presence of either 1 or 10 equiv of PPh_3. The sample was then removed from the box and opened to air. After complete oxidation of the iron(II) compound, the solutions were tested for the presence of Ph_3PO. Control reactions without iron were also carried out. Product spectra or GC retention times were compared to those of an authentic standard.

Measurement of the Solvent Contraction Correction Factor. A 5 mL sample of chloroform at 25 °C was accurately measured and placed in a narrow tube. The volume of this sample was determined at 5 °C temperature intervals between +25 and −45 °C and converted to density values on the basis of the mass of the sample. A linear least-squares regression analysis of these data provided the temperature dependence of the solvent contraction.[48]
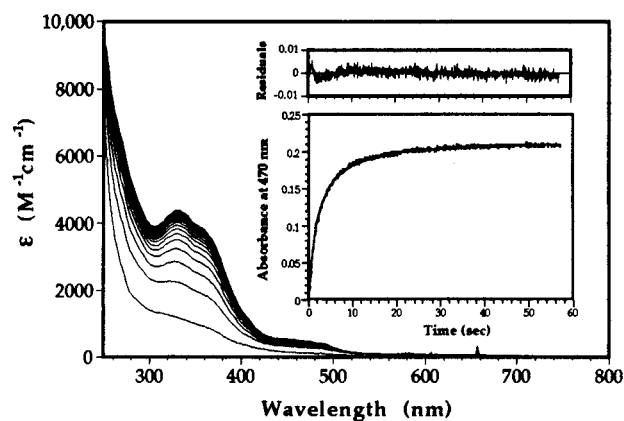
---

(47) *Oxygen and Ozone*; Battino, R., Ed.; Pergamon Press: Oxford, 1981; Vol. 7.
(48) Karlin, K. D.; Wei, N.; Jung, B.; Kaderli, S.; Niklaus, P.; Zuberbühler, A. D. *J. Am. Chem. Soc.* **1993**, *115*, 9506−9514.

Figure 1. Spectral transformation during the reaction of 0.30 mM **1a** with dioxygen (5.7 mM) in $CHCl_3$ at 22 °C. The inset shows a kinetic trace obtained from a similar run collected at 470 nm. A fit to eq 4 is superimposed on the experimental data, and the residual absorbance is shown.

Computer Modeling. The tetranuclear transition state proposed for the reaction of **2a** with dioxygen was modeled by using the CAChe MM2 package.[49] Initial structural parameters for the dinuclear domain were based on the crystal structure of the (μ-oxo)diiron(III) species **2b**. The peroxide O−O and the Fe−O_{peroxo} initial bond length parameters were based on the X-ray structure of $[Fe_6(O_2)(O)_2(OBz)_{12}$-$(H_2O)_2]$ (**3**),[50] following which the Fe−O−O−Fe dihedral angle was artificially set at 0, 45, or 90°. Energy minimization cycles were computed from each of these starting points, fixing the dihedral angle so that it could vary by no more than 10° from the initial setting.

Results

Reaction of 1a with Dioxygen in Chloroform. The stoichiometry of the conversion of **1a** into **1b** by dioxygen has been previously determined to be that shown in eq 1.[41] When chloroform solutions of **1a** and O_2 were mixed, a green-brown product appeared rapidly, the absorption spectrum of which corresponds to **1b**. This spectral transformation is shown in Figure 1. The buildup of the oxo-bridged complex was followed at 470 nm, a wavelength where only the product absorbs.[41]

Reaction Order with Respect to the Complex. The initial rate of the reaction (V_0) can be calculated from a kinetic trace based on eq 3. A plot of $\ln(V_0)$ versus $\ln([\mathbf{1a}])$ for data collected

$$V_0 = \mathrm{d}(A_t/\epsilon_0)/\mathrm{d}t = k[\mathbf{1a}]^n \qquad (3)$$

at 22 °C between 0.12 and 0.64 mM **1a** in the presence of large excesses of dioxygen (5.7 mM) is shown in Figure 2. Analysis of this plot yields a reaction order of 2.0 ± 0.1 with respect to the diiron(II) complex. The rate constant at each of these conditions is provided in Table S1 in the Supporting Information. The data were mathematically fit to an expression of an integrated second-order buildup (eq 4) using up to 1000 experimental points per kinetic trace. A typical trace and the calculated fit are shown in the inset to Figure 1.

$$A_t = A_\infty - [\Delta A^{-1} + 2k_{\mathrm{obs}}\Delta\epsilon^{-1}t]^{-1} \qquad (4)$$

In eq 4, A_t and A_∞ are the measured absorbancies at time t and after completion of the reaction, ΔA is the absorbance change during the reaction, and $\Delta\epsilon$ is the difference between

---

(49) *CAChe*; Tektronix: Beaverton, OR, 1991.
(50) Micklitz, W.; Bott, S. G.; Bentsen, J. G.; Lippard, S. J. *J. Am. Chem. Soc.* **1989**, *111*, 372−374.
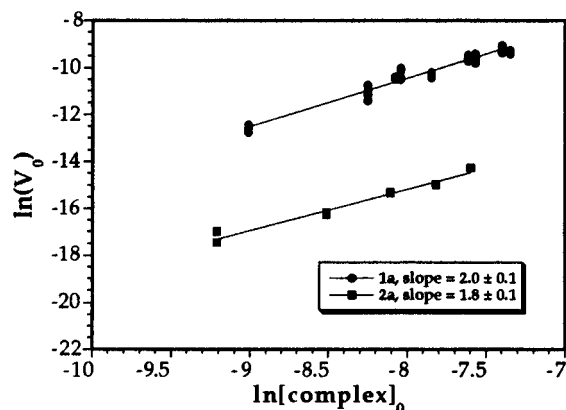
Figure 2. $\ln(V_0)$ versus the $\ln([\text{complex}]_0)$ for reactions of **1a** and **2a** with dioxygen in CHCl$_3$. Linear least-squares fits (solid lines) are superimposed upon the experimental data, the slope of which equals the reaction order. Experimental data are provided in Tables S1 and S2.
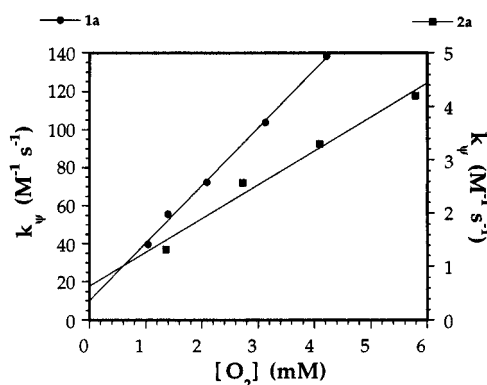

Figure 3. k_ψ versus [O$_2$] for reactions of **1a** and **2a** with dioxygen in CHCl$_3$. Data were collected at 22 °C. Linear least-squares fits (solid lines) are superimposed upon the experimental data. Experimental data are provided in Tables S3 and S4.

the extinction coefficients of the reactants and products. The only absorbing species at 470 nm is the product **1b**, the molar absorptivity of which was determined to be 657 ± 10 M^{-1} cm^{-1}, in reasonable agreement with the published value of 680 M^{-1} cm^{-1} at 478 nm.[41] Values for the extinction coefficients given here are per dinuclear molecule.

Reaction Order versus Dioxygen. The saturation concentration of dissolved dioxygen in chloroform is 11.48 mM at 20 °C.[47] In a stopped-flow experiment using a 1:1 ratio of the reaction components, however, the maximum accessible concentration of O$_2$ is only 5.74 mM after mixing since the diiron-(II) solution must be free of dioxygen. Lower dioxygen concentrations, down to around 1.4 mM, were achieved by mixing N$_2$ and O$_2$ prior to dissolution in chloroform. Since the concentration of dioxygen greatly exceeded that of the diiron complex in all the experiments, it was approximated as a constant throughout the reaction. A plot of k_ψ versus [O$_2$] (Figure 3) is linear, indicating a reaction order of 1. The small positive intercept (10 ± 2), if significant, might indicate the presence of a reversible step prior to dioxygen binding. Internal rearrangements required to provide dioxygen binding sites, observed in other reactions of this type, might account for such behavior.[24,36] A plot of $\ln(k_{1a})$ versus $\ln([\text{O}_2])$ is also linear and has a slope of 0.96 ± 0.10, confirming that the reaction is first-order in dioxygen. Rate constants are provided in Table S3 in the Supporting Information. The complete rate law for the oxidation of **1a** by dioxygen in chloroform is therefore given by eq 5. The reaction is third-order overall, the rate constant
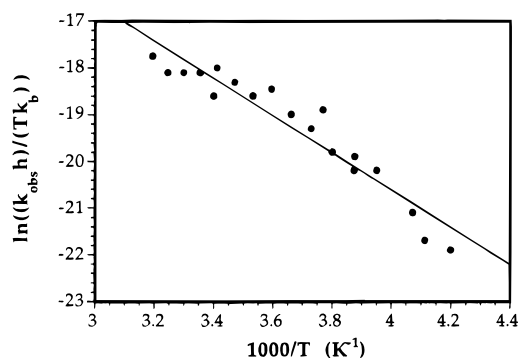

Figure 4. Eyring analysis for reaction of 0.3 mM **1a** with excess O$_2$ in CHCl$_3$ between -35 and $+40$ °C. Experimental data are provided in Table S5.

being $(4.8 \pm 0.9) \times 10^4$ M^{-2} s^{-1} at 22 °C.

$$-\frac{\text{d}}{\text{d}t}[\mathbf{1a}] = -\frac{2\text{d}}{\text{d}t}[\text{O}_2] = 2k_\psi[\mathbf{1a}]^2 = 2k_{\mathbf{1a}}[\text{O}_2][\mathbf{1a}]^2 \quad (5)$$

Activation Parameters. Kinetic data were collected over a 75 °C temperature range to determine the activation parameters for the reaction of **1a** with O$_2$ (Table S5 in the Supporting Information). Since chloroform contracts significantly over this range, a correction factor was applied on the basis of the approximation that the solvent density varies linearly with temperature (Figure S1 in the Supporting Information). The experimentally determined equation for the density of chloroform as a function of temperature and the corresponding adjustment to the dissolved dioxygen concentration are given in eqs 6 and 7, respectively. Figure 4 shows an Eyring analysis of the data. The derived activation parameters are listed in Table 1, together with some values for similar dinuclear iron complexes.

$$\rho_T = 1.520(1) - 0.0018(1)T \quad (T \text{ in } °C) \quad (6)$$

$$[\text{O}_2]_T = [\text{O}_2]_{22\,°C}\,\rho_{22\,°C}^{-1}\,\rho_T \quad (7)$$

At no time during the course of this reaction was an intermediate observed by optical spectroscopy. In freeze-quench experiments, however, a signal indicative of a mixed-valent species was previously reported during oxidation of **1a** in CH$_2$Cl$_2$.[41] In these experiments, the samples were frozen approximately 30 s after exposure to air at -78 °C. From the activation parameters measured here and the concentrations used in the EPR experiments (1.7–5.5 mM) the half-life under these conditions can be estimated to be approximately 5–6 min. Whether or not the EPR signal corresponds to a species along the oxidation pathway will be further discussed below.

Stoichiometry of the Reaction of 2a with Dioxygen. Oxidation of **2a** yields the (μ-oxo)bis(μ-carboxylato)diiron(III) complex **2b**.[42] The stoichiometry of this reaction was determined by manometry in both methanol and chloroform. Oxidation of 1 mol of the diferrous compound consumed 0.5 ± 0.1 mol of dioxygen in both solvents, and the reaction proceeds as indicated in eq 2. These results show that, as for **1a**, all the oxidizing equivalents of molecular oxygen are consumed in converting diiron(II) to the (μ-oxo)diiron(III) core. Equation 2 further suggests that 1 equiv of hydroxide is generated in the oxidation reaction. Resonance Raman experiments using ^{18}O$_2$ have verified that the oxygen atom of **2b** derives from dioxygen and not from the bridging hydroxide ligand of the starting material (Figure 5). Since OH$^-$ is generated in the reaction, we tested to see whether free hydroxide exchanges with the

Table 1. Activation Parameters for Reactions of **1a** and Similar Compounds with Dioxygen

compound	temperature range (°C)	$\Delta H^{\ddagger}$ (kJ mol^{-1})	$\Delta S^{\ddagger}$ (J mol^{-1} K^{-1})	$\Delta G^{\ddagger}_{293}$ (kJ mol^{-1})	ref
1a[a]	−35 to +40	33 ± 2	−39 ± 9	44 ± 10	this work
[(Fe$_2$(HPTMP)(OBz)](BF$_4$)$_2$[b]	−5 to +35	113 ± 8	187 ± 27	58 ± 9	24
[(Fe$_2$(HPTP)(OBz)](BF$_4$)$_2$[b]	−68 to +25	52 ± 3	−47 ± 11	66 ± 16	24
[(Fe$_2$(EtHPTB)(OBz)](BF$_4$)$_2$[b]	−5 to +25	81 ± 4	74 ± 14	59 ± 11	24

[a] The errors reported here are based on the curve fitting as defined in the text. Because of the curvature of the plot, the actual error may be slightly greater. [b] Values are for the decay of the observed peroxide intermediate.
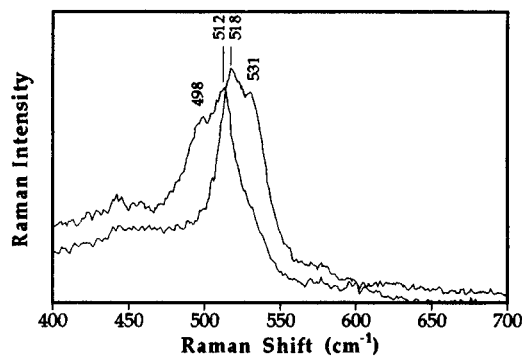

Figure 5. Resonance Raman spectra (406.7 nm irradiation) of **2b** (~2 mM) from reaction of **2a** with $^{16}O_2$ and $^{18}O_2$ in MeOH. Peaks at 531 and 518 cm^{-1} correspond to the $^{16}O_2$ sample, and the features at 512 and 498 cm^{-1} arise from the $^{18}O_2$ species.

μ-oxo ligand. Addition of several drops of 2 M NaOH solution to [^{18}O]**2b** resulted in no exchange of the oxo bridge. Addition of water, on the other hand, is an effective method of exchanging the bridging atom in (μ-oxo)diiron(III) complexes.[51] Interestingly, the symmetric Fe−O−Fe vibration, which occurs in the frequency region expected for a tribridged (μ-oxo)diiron(III) compound,[22,52] appeared as a doublet in both the ^{16}O and ^{18}O samples, at 531, 518 and 512, 498 cm^{-1}, respectively. This splitting appears in the solid state spectrum[53] as well as in the solution spectra presented here. Since the feature is present in both states, it probably arises from the coupling of the Fe−O−Fe symmetric stretch with another vibration in the molecule.

Kinetics of the Reaction of 2a with Dioxygen in Chloroform. The oxidation of **2a** to **2b** was followed spectrophotometrically in a manner similar to that for **1a**. Figure 6 displays the spectral changes that accompany this transformation. Kinetic traces were recorded at 474 nm. The reaction in CHCl$_3$ exhibits a second-order dependence on the concentration of the diferrous compound (Figure 2) and a first-order dependence on dioxygen concentration (Figure 3). The complete rate law for the oxidation of **2a** to **2b** is given by eq 8. Under conditions

$$\text{rate}_{\text{CHCl}_3} = \frac{d[\mathbf{2b}]}{dt} = 2k_{\psi}[\mathbf{2a}]^2 = 2k_{\mathbf{2a}}[O_2][\mathbf{2a}]^2 \qquad (8)$$

of excess O$_2$, a third-order rate constant, $k_{\mathbf{2a}} = 460 \pm 90$ M^{-2} s^{-1}, was obtained. An extinction coefficient of 1200 ± 20 M^{-1} cm^{-1} in chloroform was determined from the fitting parameters as described for **1b.** Previously published values for the extinction coefficient of **2b** were significantly dependent on the counterion and solvent, and include $\epsilon_{475} = 1560$ M^{-1} cm^{-1} for the hexafluorophosphate salt in water and $\epsilon_{472} = 1450$ M^{-1} cm^{-1} for the perchlorate salt in methanol.[42]

Observation of Intermediates. Figure 7 shows the time-dependent spectral changes in the 500−800 nm region for the reaction of **2a** with dioxygen. A small but reproducible broad

Figure 6. Spectral transformation during reaction of 0.20 mM **2a** with dioxygen (5.3 mM) in MeOH at 22 °C. The inset shows a kinetic trace obtained from a similar run collected at 474 nm with the single-wavelength equipment. A fit to eq 4 is superimposed on the experimental data, and the residual absorbance is shown. The spectral transformation in MeOH is the same as that in CHCl$_3$.
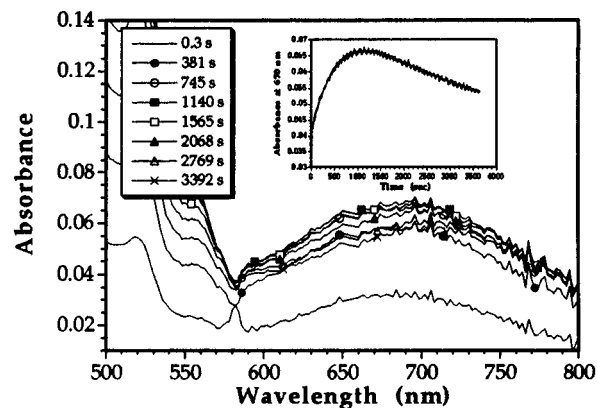
Figure 7. Expanded view of the optical spectrum of an intermediate during reaction of **2a** (0.50 mM) with dioxygen (1.2 mM) in CHCl$_3$ at 22 °C. The inset trace shows the absorbance at 670 nm as a function of time. Superimposed on these data (solid line) is a least-squares fit.

feature grew in and then decayed. Dinuclear iron−peroxide adducts exhibit a charge transfer band around 600 nm.[15,36,54−57] Unfortunately, the product **2b** absorbs in this region, which complicates data analysis. Attempts to use global analysis to deconvolute the spectral changes were unsuccessful owing to the small optical density changes. By extracting single-wavelength data at 670 nm, the complicated line shape could be fit to a sum of a second-order growth and a first-order decay. The growth phase at 670 nm had a rate constant comparable to that of the 470 nm band under similar conditions, but the error

(51) Armstrong, W. H.; Spool, A.; Papaefthymiou, G. C.; Frankel, R. B.; Lippard, S. J. *J. Am. Chem. Soc.* **1984**, *106*, 3653.

(52) Sanders-Loehr, J.; Wheeler, W. D.; Shiemke, A. K.; Averill, B. A.; Loehr, T. *J. Am. Chem. Soc.* **1989**, *111*, 8084−8093.
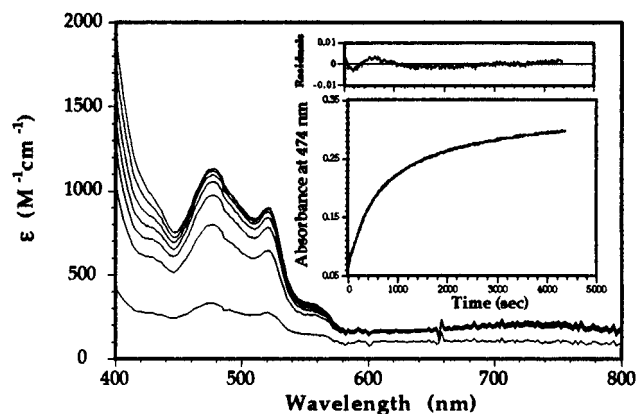
(53) Sanders-Loehr, J. Personal communication.

(54) Dong, Y.; Menage, S.; Brennan, B. A.; Elgren, T. E.; Jang, H. G.; Pearce, L. L.; Que, L., Jr. *J. Am. Chem. Soc.* **1993**, *115*, 1851−1859.

(55) Kitajima, N.; Tamura, N.; Amagai, H.; Fukui, H.; Moro-Oka, Y.; Mizutani, Y.; Kitagawa, T.; Methur, R.; Heerwegh, K.; Reed, C. A.; Randall, C. R.; Que, L., Jr.; Tatsumi, K. *J. Am. Chem. Soc.* **1994**, *116*, 9071−9085.

(56) Kitajima, N.; Fukui, H.; Moro-oka, Y.; Mizutani, Y.; Kitagawa, T. *J. Am. Chem. Soc.* **1990**, *112*, 6402−6403.

(57) Moro-Oka, Y.; Fujisawa, K.; Kitajima, N. *Pure Appl. Chem.* **1995**, *67*, 241−248.

Scheme 1
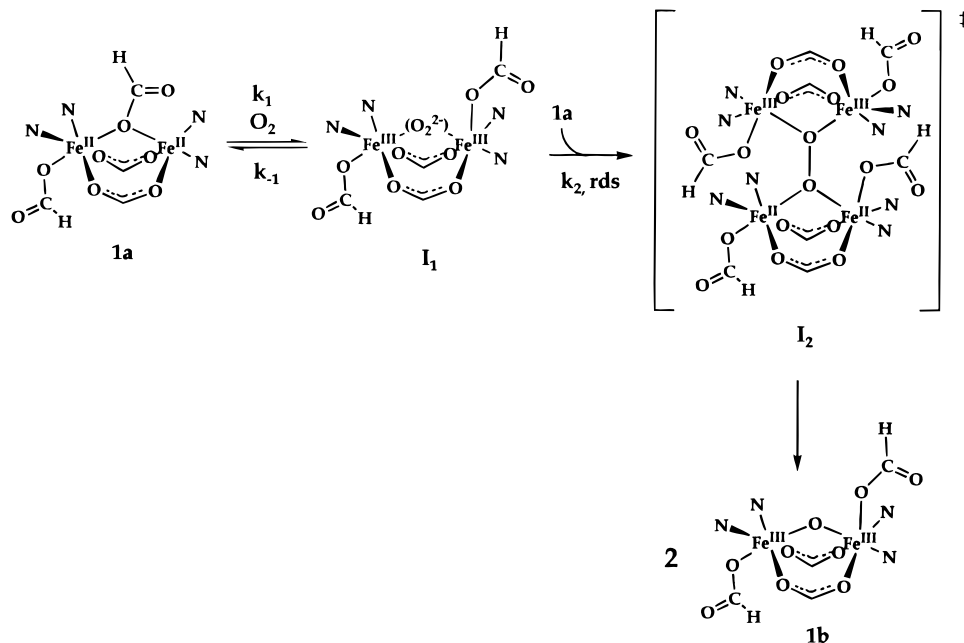
values for these rates derived from the curve fitting were sizable owing to the large number of independent variables required for the fitting.

NMR Spectral Evidence for Carboxylate Ligand Exchange. Both of the iron atoms in **2a** are coordinatively saturated. If the reaction of this complex with dioxygen were to proceed by an inner-sphere mechanism, a site for O_2 coordination would have to be available. A likely route for this process is by a carboxylate shift, in which one of the bidentate bridging acetates becomes a monodentate terminal ligand.[58] Variable temperature ^1H and ^2H NMR studies were therefore carried out in order to determine whether the carboxylate bridges exchange with free acetate in solution at a rate that is fast with respect to the observed oxidation. Complete exchange can be considered an extreme case of carboxylate shifting, and a monodentate−bidentate shift must be as fast or faster than such a substitution reaction. The addition of sodium acetate-d_3 to **2a** resulted in the loss of the broad ^1H signal at ~23 ppm ($T = -30$ °C) associated with bound acetate, indicating it to be in rapid exchange with free ligand. Concomitantly, a resonance at ~23 ppm appeared in the ^2H spectrum. As the temperature was raised above −30 °C, broadening of the free and bound acetate-d_3 signals occurred, although coalescence of these resonances did not take place at temperatures up to 60 °C. The temperature-dependent ^2H spectra are shown in Figure S2 in the Supporting Information. Similar carboxylate ligand exchange was identified for **1a** in a previous study.[41]

Addition of Triphenylphosphine. Triphenylphosphine, a good acceptor in oxo-transfer reactions,[59] was added to test for the possible formation of a high-valent oxo (ferryl or perferryl) intermediate. No such species could be trapped. Triphenylphosphine oxide was not detected by gas chromatography or by ^{31}P NMR spectroscopy in reactions of **1a** or **2a** with dioxygen.

Discussion

Mechanistic Consideration of the Reaction of [Fe₂-(BIPhMe)₂(O₂CH)₄] (1a) with Dioxygen. The primary feature

(58) Rardin, R. L.; Tolman, W. B.; Lippard, S. J. *New J. Chem.* **1991**, *15*, 417−430.

(59) Holm, R. H.; Donahue, J. P. *Polyhedron* **1993**, *12*, 571−589.

of the reaction with dioxygen is the second-order dependence on the concentration of the diiron(II) species. Several years ago, solely on the basis of stoichiometric results, a mechanism was proposed for this oxidation reaction, the key feature of which was a tetranuclear intermediate.[41] The present kinetic data strongly support many aspects of this earlier proposal.

Two general reaction schemes fit the data. The first, and more probable, one consists of dioxygen reacting reversibly with the diferrous compound to form an intermediate, $\mathbf{I_1}$. This intermediate then reacts with another equivalent of the starting material to afford the product, probably passing through a tetranuclear transition state, $[\mathbf{I_2}]^{\ddagger}$. The latter collision is the rate-determining step and $[\mathbf{I_2}]^{\ddagger}$ rapidly decomposes into 2 equiv of product (eq 9). The rate law corresponding to this sequence is given in eq 10 and reverts to the observed rate law under

$$\mathbf{1a} + O_2 \underset{k_{-1}}{\overset{k_1}{\rightleftharpoons}} \mathbf{I_1} \overset{+\mathbf{1a}}{\underset{k_2}{\longrightarrow}} 2(\mathbf{1b}) \tag{9}$$
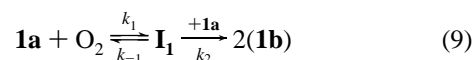
$$\frac{d[\mathbf{1b}]}{dt} = 2k_{\psi}[\mathbf{1a}]^2 = \frac{2k_1 k_2 [\mathbf{1a}]^2 [O_2]}{k_{-1} + k_2[\mathbf{1a}]} \tag{10}$$

conditions where $k_{-1} \gg k_2[\mathbf{1a}]$. Another kinetically indistinguishable reaction scheme has two molecules of **1a** colliding to form a tetranuclear iron(II) species which then reacts with a dioxygen molecule (eq 11). We prefer the mechanism depicted in eq 9, however, since it is chemically more reasonable and because other diiron(II) compounds react similarly.[24,36]

$$2(\mathbf{1a}) \underset{k_{-1}}{\overset{k_1}{\rightleftharpoons}} \mathbf{I} \overset{+O_2}{\underset{k_2}{\longrightarrow}} 2(\mathbf{1b}) \tag{11}$$
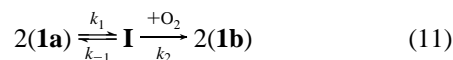
A chemical interpretation of the pathway from eq 9 is given in Scheme 1. This proposed mechanism differs from that suggested previously[41] in that the initial reaction with dioxygen is reversible and oxo transfer to substrate is now omitted. Intermediate $\mathbf{I_1}$ does not appear to have the power to oxidize even the very efficient oxo acceptor Ph₃P. Finally, the two reaction schemes differ in the oxidation states of iron. In the original scheme, the dioxygen binding step was proposed to be accompanied by one-electron transfer, forming a superoxide adduct. This assignment was based on the observation of an

EPR signal as discussed above. I_1 was drawn in Scheme 1 as a diferric peroxide in analogy to the reactions of other diiron-(II) systems with dioxygen.[54,56,60,61] Three examples of these species have now been crystallographically characterized.[25,26,28] Two-electron processes clearly seem to dominate the O_2 reactivity of both diiron(II) model compounds and proteins. Optical absorption in the 600−700 nm region, characteristic of such adducts, has not been observed during reactions of **1a** with dioxygen, but its absence could be the result of low steady-state concentrations. Rapid interconversion between I_1 and the mixed-valent superoxide adduct is most likely responsible for the observed EPR signal following freeze quenching, although we cannot completely exclude the possibility that I_1 is itself the mixed-valent superoxo species.

A point of interest concerning compound **1a** is whether or not an open site exists for dioxygen binding. Strictly speaking, this complex has a vacant coordination site on one of the iron atoms, as revealed by the X-ray structure. In early studies of **la** attempting to mimic the anion binding behavior of metHr, the complex was allowed to react with a variety of potential ligands.[41] No coordination of an anionic or neutral ligand was observed. This behavior was ascribed to a steric hindrance of the "pentacoordinate" iron atom by the dangling oxygen atom of the monodentate formate ligand.

Even though added ligands do not appear to bind to **1a**, carboxylate exchange reactions are facile. The concept of the carboxylate shift was developed in part because **1a** rapidly exchanged its formate bridges with added carboxylates, $R'CO_2$-Na.[41,58] This exchange presumably passed through an intermediate monodentate state, which is susceptible to replacement by an incoming ligand. Such shifting of the carboxylate is also invoked in the oxidation mechanism. A shift from a bridging to terminal coordination is proposed to allow dioxygen adduct formation (I_1). An analogous shift is required in the product-forming step k_2.

The temperature dependence for the reaction of **1a** with O_2, Figure 4, yields $\Delta H^\ddagger = 33 \pm 2$ kJ mol^{-1} and $\Delta S^\ddagger = -39 \pm 9$ J mol^{-1} K^{-1}. These are composite values, containing contributions from the three elementary reactions characterized by rate constants k_1, k_{-1}, and k_2. On closer inspection, the deviations from the line in Figure 4 at the high- and low-temperature extremes appear to be systematic, possibly indicating a change in the rate-determining step with a change in temperature. There is a realistic possibility that the carboxylate shift is no longer "fast" relative to the subsequent steps at the lowest temperatures employed.

Given the large scatter in the data, a separate analysis of the high- and low-temperature regimes did not seem warranted. Also, we note that the kinetic traces appeared strictly second-order throughout. Had the rate-determining step changed completely from a second-order reaction of Scheme 1 ($k_2[I_1]$-[**1a**]) to a first-order carboxylate shift, the kinetic order in [**1a**] would have changed from 2 to 1. Because this change did not occur, and because there is only a hint of curvature in Figure 4, we conclude that, at best, only minor mechanistic adjustments take place in the temperature range examined.

The formation of polynuclear peroxo intermediates is well documented in the literature of iron(II)−porphyrin systems,[62−65]

and a diiron(III) peroxo intermediate in the pathway of sMMO hydroxylase has recently been identified.[61] A non-heme polyiron peroxide compound has also been structurally characterized, $[Fe_6(O_2)(O)_2(OBz)_{12}(H_2O)_2]$ (**3**), and is depicted below.[50]
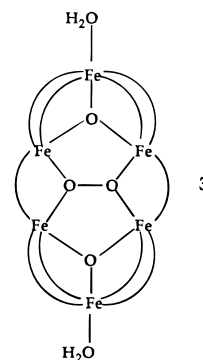
This complex has an in-plane $\mu,\mu\text{-}\eta^2\text{:}\eta^2$-peroxide ligand linking four ferric ions. Synthesized by addition of hydrogen peroxide to basic iron benzoate, the core of this complex is presumably stabilized toward reductive cleavage of the O−O bond because the ferric ions cannot be easily oxidized to iron(IV). The structure of the proposed transition state $[I_2]^\ddagger$ in Scheme 1 is similar to that of the $\{Fe^{III}_4O_2\}$ core in **3**, the existence of which lends credence to our hypothesis. Since the proposed unstable species contains two ferric ions and two ferrous ions, in contrast to the tetraferric center in **3**, rapid O−O bond homolysis is expected with concomitant oxidation of the two iron(II) ions. Unfortunately, O−O bond cleavage occurs after the rate-determining step, so the present kinetic data do not provide conclusive information regarding this process.

Mechanistic Consideration of the Reaction of [Fe$_2$(OH)-(Me$_3$TACN)$_2$(OAc)$_2$](ClO$_4$) (2a) with Dioxygen. The results for the oxidation of **2a** in chloroform are consistent with a mechanism analogous to that proposed for the reaction of **1a** with dioxygen (eq 9 and Scheme 1). Dioxygen reacts with the dinuclear iron(II) compound, forming a peroxodiiron(III) intermediate which then reacts with another equivalent of the ferrous precursor. One major difference between **1a** and **2a** is the saturated coordination environment of **2a**. Although 7-coordinate iron compounds are known, they are rare. It is more likely, therefore, that the addition of dioxygen to the metal center is preceded by a unimolecular rearrangement leading to an open coordination site. A carboxylate shift transforming one of the bridging carboxylates into a monodentate carboxylate is the most likely rearrangement. Recent work has addressed the role of solvents in carboxylate shift reactions. Polar protic solvents such as methanol favor monodentate coordination.[66] Oxidation of **2a** by O_2 is indeed faster in methanol than in CHCl$_3$,[67] consistent with this proposal.

Results of a computer modeling study of the transition state $[I_2]^\ddagger$ proposed for the reaction of **2a** with O_2 are shown in Figure 8. The question was whether such a tetranuclear species could form owing to potential steric contacts between the methyl groups on the Me$_3$TACN ligand. The absolute energy values from MM2 calculations of this type are not accurate because

(60) Hayashi, Y.; Suzuki, M.; Uehara, A.; Mizutani, Y.; Kitagawa, T. *Chem. Lett.* **1992**, 91−94.

(61) Liu, K. E.; Valentine, A. M.; Qiu, D.; Edmondson, D. E.; Appelman, E. H.; Spiro, T. G.; Lippard, S. J. *J. Am. Chem. Soc.* **1995**, *117*, 4997−4998.

(62) Balch, A. L. *Inorg. Chim. Acta* **1992**, *198*−200, 297−307.

(63) Balch, A. L.; Chan, Y.-W.; Cheng, R.-J.; La Mar, G. N.; Latos-Grazynski, L.; Renner, M. W. *J. Am. Chem. Soc.* **1984**, *106*, 7779−7785.

(64) Chin, D.-H.; Del Gaudio, J.; La Mar, G. N.; Balch, A. L. *J. Am. Chem. Soc.* **1977**, *99*, 5486−5488.

(65) Chin, D.-H.; La Mar, G. N.; Balch, A. L. *J. Am. Chem. Soc.* **1980**, *102*, 4344−4350.

(66) Connolly, J. A.; Kim, J. H.; Banaszczyk, M.; Drouin, M.; Chin, J. *Inorg. Chem.* **1995**, *34*, 1094−1099.

(67) Feig, A. L.; Lippard, S. J. Unpublished results.
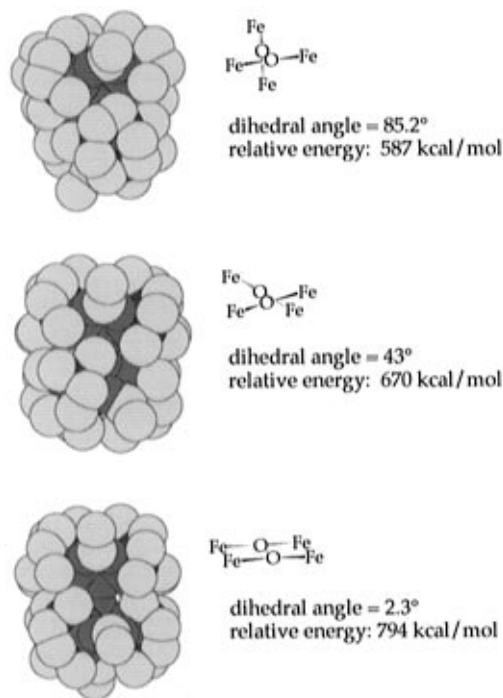
Figure 8. Results of CACHe molecular modeling of the $[\mathbf{I_2}]^{\ddagger}$ transition state for the reaction of **2a** with O_2. Space-filling diagrams are oriented such that the O–O bond lies vertically in the plane of the page.

of inadequacies in the force field, but relative values do provide some measure of the favored states. The three structures depicted in Figure 8 differ mainly in the Fe–O–O–Fe dihedral angle, the other geometric parameters being similar for the minimized structures. The calculations show only one orientation of the Fe_2OOFe_2 core, that with an Fe–O–O–Fe dihedral angle of approximately 90°, to be reasonable. The other structures have unfavorable nonbonded contacts. In all three minimized structures, the O–O bond distance refined to 1.60 Å, and fixing a shorter bond length of 1.48 Å resulted in higher energy species. Since this complex is proposed to be a transition state on the path to O–O bond cleavage, the elongated bond was considered to be reasonable.

A variable temperature NMR study of **2a** (Figure S2) supports the idea of solvent-assisted equilibria. As explained above, carboxylate exchange can be considered an extreme case of carboxylate shifting. The component steps in exchange of a bidentate bridging carboxylate consist of breaking and forming the two Fe–O bonds. The carboxylate shift, however, must be at least as fast as ligand substitution. The slow exchange region can be monitored at low temperature in methanol, and at room temperature the reaction is in the intermediate exchange region on the NMR time scale. These results show that, at room temperature and above, the carboxylate shift is fast relative to the formation of **2b**. At −30 °C and below the exchange is frozen out.

An intermediate in the reaction of **2a** with dioxygen was observed spectroscopically, but proved difficult to characterize. It appeared in chloroform solutions as a green transient. The absorption maximum occurs at approximately 670 nm, a region associated with peroxide-to-iron(III) charge-transfer bands.[26,54−56,60,61] The weakness of the signal could result from either the low concentration of the chromophore or a small extinction coefficient. The former is more likely since all known non-heme peroxodiiron(III) complexes with absorption features in this region have extinction coefficients between 1000 and 2000 M^{-1} cm^{-1}.[54−56,60] Attempts to observe ν_{O-O} in the

resonance Raman spectrum by exciting time-resolved or freeze-quenched samples at 647.1 nm were unsuccessful.

Recently, the asymmetric, coordinatively unsaturated compound $[Fe_2(O)(OAc)_2(Me_3TACN)(bpy)](PF_6)_2$ was reported to have catalase activity.[68] The structure of the proposed diiron-(III) peroxo intermediate in that study is quite similar to that of $\mathbf{I_1}$. Compound **2b** was not capable of disproportionating hydrogen peroxide under the same conditions, however, because it is coordinatively saturated.[68] The results clearly indicate the need for a vacant site(s) at the dinuclear iron center to bind O_2 or H_2O_2. Without such a vacancy, intermediates involving carboxylate shifts will probably be required.

Comparison of Kinetic Results for the Two Compounds. The reactions of **1a** and **2a** with dioxygen are remarkably similar. Both traverse a polynuclear iron–peroxide transition state on their way to the (μ-oxo)diiron(III) products. When studied under a narrow set of conditions, the reactions appear quite simple. As the temperature-dependent studies indicate, however, they are more complex.

In Scheme 1, we have assumed oxidation of iron by an inner- rather than an outer-sphere electron-transfer mechanism. This mechanism is indicated by the complex kinetic behavior and by the complete incorporation of isotopic label into the oxo bridge when $^{18}O_2$ is employed. Outer-sphere mechanisms have been proposed for the autoxidation of several mononuclear iron-(II) model compounds.[69]

The mechanisms presented for oxidation of **1a** and **2a** are also comparable to those deduced from studies of iron(II)–porphyrin complexes with dioxygen, where diferric porphyrinato–peroxo complexes have been observed.[63−65,70] Here, O–O bond cleavage yields ferryl species as intermediates. The failure to oxidize PPh_3 in the present system strongly argues against the involvement of ferryl or perferryl species. The lifetimes of these intermediates would have to be exceedingly short to subvert oxo-transfer chemistry. The mechanism presented in Scheme 1, in which O–O bond cleavage affords the (μ-oxo)diiron(III) products directly, is therefore preferred.

Implications for Non-Heme Iron Enzymes. The two complexes studied here react with dioxygen by a pathway that clearly is inaccessible to the enzyme systems. The initial dioxygen binding step is related to the formation of intermediates like H_{peroxo} in the sMMO hydroxylase system,[71] but a cascade of reactions involving the formation of polynuclear iron species rapidly ensues in the case of the model compounds. Proteins prevent such reactions kinetically by sequestering the diiron center deep within the folded polypeptide. In this manner, slower reactions leading to substrate activation become dominant. The intermediate observed in the reaction of **2a**, tentatively assigned as a diferric peroxide, is long-lived for a species of this type. The low steady-state concentration, due to the presence of a rapid back-reaction, makes it difficult to study, however.

The kinetic results strongly imply a role for carboxylate shifts in controlling the behavior of the oxidation reactions. It is likely that similar dissociative steps are involved in the protein systems. Since dioxygen reactivity can be tailored so dramatically by this phenomenon, it appears to be an ideal mechanism for the biological control of active site reactivity. Carboxylate shifts

(68) Mauerer, B.; Crane, J.; Schuler, J.; Wieghardt, K.; Nuber, B. *Angew. Chem., Int. Ed. Engl.* **1993**, *32*, 289−231.

(69) Sauer-Masarwa, A.; Herron, N.; Fendrick, C. M.; Busch, D. H. *Inorg. Chem.* **1993**, *32*, 1086−1094.

(70) Balch, A. L.; La Mar, G. N.; Latos-Grazynski, L.; Renner, M. W.; Thanabal, V. *J. Am. Chem. Soc.* **1985**, *107*, 3003−3007.

(71) Liu, K. E.; Valentine, A. M.; Wang, D.; Huynh, B. H.; Edmondson, D. E.; Salifoglou, A.; Lippard, S. J. *J. Am. Chem. Soc.* **1995**, *117*, 10174−10185.

could arise from the binding or dissociation of other protein components, such as protein B or reductase in the sMMO system, substrate, or other allosteric effectors. The role of the coupling protein in sMMO is still not known, but the proposed binding site, based on the crystal structure of the hydroxylase component, is ideally suited for such a regulatory role. Situated along helices E and F of the canyon, binding of protein B would be readily transmitted to the diiron center through helix motion. Further studies with the enzyme system are addressing these issues. Already, several carboxylate shift motifs have been observed in sMMO hydroxylase crystals by varying the crystallization conditions.[21,72]

Implications for Modeling Studies. The present experiments strongly argue that proper design of biomimetic models for diiron(II) oxygen activating proteins must take into account the need to block bimolecular reactions of the core. Such processes have been avoided, or at least diminished, in some model systems by using ligands bulkier than BIPhMe or Me_3TACN.[26,54-56,60] The use of more sterically hindered ligands is clearly a step in the proper direction, and a kinetic study of three such complexes is presented elsewhere.[24] In these systems, greater stability of the peroxide intermediates is achieved and the separation of the two kinetic steps is possible. A further step toward minimizing bimolecular decay of the intermediates could be achieved by immobilization of the ferrous material on a solid support. By sequestering the dinuclear center in this way, second-order reactions would be eliminated without preventing access of a potential substrate. Such studies would more accurately reflect the role of the protein without resorting to elaborate ligand design.

Another possibility is to run the reactions in more viscous solvents, which may decelerate bimolecular reactions that lead to the decay of the peroxide intermediates. Under such conditions, potential unimolecular pathways may form different intermediates which might be capable of carrying out oxo-transfer reactions.

Conclusions

This work provides kinetic and mechanistic analyses of the reaction of dioxygen with two dinuclear non-heme iron protein models. Despite structural similarities with the protein cores, an alternative reaction ensues for these compounds. The first step involves dioxygen binding to a vacant coordination site, made available by a carboxylate shift reaction. Cleavage of the O−O bond occurs after the rate-determining formation of a tetranuclear peroxide transition state. An intermediate has been observed in the oxidation of **2a**.

Supporting Information Available: Tables S1−S5, containing kinetic constants used to prepare the figures and Figures S1 and S2 (8 pages). See any current masthead page for ordering and Internet access instructions.

JA962814E

(72) Rosenzweig, A. C.; Frederick, C. A.; Lippard, S. J. In *Microbial Growth on C₁ Compounds: Proceedings of the 8th International Symposium*; Lidstrom, M. E., Tabita, F. R., Eds.; Kluwer Academic Publishers: Dordrecht, The Netherlands, 1996; pp 141−149.